Current Chemistry Letters 15 (2026) 533–544

Contents lists available at GrowingScience

Current Chemistry Letters

homepage: www.GrowingScience.com

Theoretical investigation of N-fused heterocyclic small-molecule donors end-capped with 2-(2-thienylmethylene)malononitrile for organic solar cells

Ikram Mennas[a*], Jaouad Ouhrira[a,b], Yahya Mekaoui[b], Redouan Elharkaoui[a], El Mostafa Benharafa[c], Mohamed Omari[a], Abdelah Zeroual[c], Bouzid Manaut[b], Mohammed El Idrissi[a*]

[a]*Team of Sustainable Processes, Advanced Materials and Computational Chemistry, Sultan Moulay Slimane University, Polydisciplinary Faculty, Beni Mellal, Morocco*
[b]*Laboratory of Research in Physics & Engineering Sciences, Sultan Moulay Slimane University, Polydisciplinary Faculty, Beni Mellal, Morocco*
[c]*Molecular Modeling and Spectroscopy Research Team, Faculty of Sciences, Chouaib Doukkali University, El Jadida, Morocco*

C H R O N I C L E

Article history:
Received January 24, 2026
Received in revised form
March 29, 2026
Accepted May 16, 2026
Available online
May 16, 2026

Keywords:
Heterocycles
Donor materials
OSCs
Open-Circuit Voltage
TD-DFT

A B S T R A C T

The design of new high-performance donor materials remains a major challenge for improving organic solar cells (OSCs). In this study, four N-fused heterocyclic small-molecule donor analogues symmetrically end-capped with 2-(2-thienylmethylene)malononitrile units were theoretically investigated by DFT and TD-DFT methods using B3LYP/6-31G(d,p) calculations, incorporating the solvent effect via the CPCM model with tetrahydrofuran (THF). The studied systems consist of a zolpidem-inspired analogue (M1), a temozolomide-inspired analogue (M2), a tryptanthrin-inspired analogue (M3), and an extended tryptanthrin-like fused analogue (M4). Their electronic, optical, and photovoltaic properties are analyzed to evaluate their suitability for OSC applications. The differences in the electronic, optical, and photovoltaic behavior of the investigated compounds mainly originate from variations in the central N-fused heterocyclic core, which modulate pi-conjugation, frontier orbital energies, charge distribution, and intramolecular charge-transfer character. The results reveal that these nitrogen heterocycles have encouraging characteristics and a great capacity for modulation. The M1 molecule is distinguished by a low band gap (1.63 eV), light absorption extending to 935 nm, and strong chemical softness (0.613 eV), promoting charge transfer, though its power conversion efficiency remains limited to 1%. In contrast, M2 exhibits the best overall efficiency (approximately 4%), due to a deeper HOMO level (-5.88 eV) leading to a high open-circuit voltage (Voc = 1.28 V). M3 presents a balanced compromise with a PCE of around 3%, while M4 combines moderate absorption and voltage for an efficiency close to 2%. This investigation highlights the strong potential of nitrogen-fused heterocycles as adjustable donor materials for the development of high-performance organic solar cells.

2026 by the authors; licensee Growing Science, Canada.

1. Introduction

The rising need for renewable energy sources results from the continuous global increase in energy demand, particularly for solar energy, since it is abundant and environmentally sustainable. From the many solar energy conversion technologies, silicon-based solar cells continue to dominate in the market due to their high efficiency and long-term stability. However, their high manufacture cost and rigidity limit their application in flexible and low-cost electronic devices[1]. New technologies based on organic donor molecules have attracted a high level of interest due to their high energy conversion efficiency, their relatively simple fabrication and the possibility of fine-tuning their electronic properties. Nevertheless, the long-term stability and the toxicity of some materials are still major challenges[2]. Organic solar cells have attracted considerable interest because their performance can be tuned through the molecular design of donor and acceptor materials[3]. Bulk heterojunction organic solar cells have attracted broad interest because of their flexibility, low material consumption, and compatibility with solution-based fabrication processes[4-6]. The bulk heterojunction architecture is particularly effective because the nanoscale donor/acceptor blend promotes exciton dissociation and charge transport. In this type of device architecture, the

* Corresponding author
E-mail address elidrissi.usms@gmail.com (I. Mennas), m.elidrissi2018@gmail.com (M. E. Idrissi)
© 2026 by the authors; licensee Growing Science, Canada
doi: 10.5267/j.ccl.2026.5.004

active layer consists of an organic donor molecule (either a small molecule or a conjugated polymer), combined with an electron acceptor, typically a fullerene derivative such as [6,6]-phenyl-C_{61}-butyric acid methyl ester (PCBM), forming a bicontinuous interpenetrating network. Upon illumination, excitons are generated in the donor phase and diffuse to the donor/acceptor (D/A) interface, where charge separation occurs. The holes are then transported through the donor phase to the corresponding electrode, while the electrons are transferred and transported within the acceptor phase formed by PCBM.[7-8] Fullerene derivatives, particularly PCBM, have long been favored as acceptors due to their high electron affinity and excellent electron mobility.[9]

An ideal donor should possess appropriate energy levels HOMO and LUMO, a high absorption coefficient, and good hole mobility.[10-12] The HOMO level must be sufficiently low to ensure a high open-circuit voltage (V_{oc}), while the LUMO must be aligned above the acceptor's LUMO to enable efficient charge separation.[9] N-fused heterocyclic donor molecules are important in the design of organic donor molecules for photovoltaic devices, in particular in organic solar cells. Their structural diversity and adjustable electronic properties enable efficient light absorption and optimal charge transport, which makes them essential components of modern photovoltaic technologies.[13-18] The incorporation of nitrogen atoms into fused-ring systems significantly enhance the stability and performance of energetic materials by introducing both σ- and π-aromaticity in five-membered heterocycles. This dual aromatic character, arising from the delocalization of nitrogen lone pairs, increases energy density through strained N-N bonds and improves thermal stability in the solid state. Molecules such as tetrazoles and pentazoles benefit from this effect, while six-membered analogs, which lack σ-aromaticity, tend to be less stable. The presence of adjacent nitrogen atoms further strengthens intermolecular interactions, boosting detonation performance, although potentially increasing sensitivity. These findings underscore the importance of balancing nitrogen content and ring size to design high-performance energetic materials. The discovery of σ-aromaticity provides a new strategy for stabilizing otherwise reactive nitrogen-rich systems.[19] While N-fused heterocycles have been extensively studied in the medical field[20], their potential in other critical areas such as energy conversion and applications in organic solar cells and optoelectronic devices remains relatively underexplored.

A novel category of donor molecules, particularly fused-ring donor molecules, has played a significant role in advancing organic solar cell (OSC) technology. These donors exhibit several chemical advantages, including an electron-rich conjugated core embedded in a modular architecture, extended π-bridges, strengthened donor units, and tunable side chains, which enable facile structural optimization. They are also characterized by relatively simple synthesis, easy purification, and good compatibility with large-scale production.

From a physical perspective, these donor molecules offer broad tunability of absorption spectra and energy levels, strong absorption in the visible and near-infrared regions, and high hole mobility. These characteristics translate into excellent device performance, including efficient charge extraction, low energy losses, high power conversion efficiencies (PCEs), and good operational stability. Optimization of donor molecules has therefore played a key role in enhancing OSC performance, contributing to power conversion efficiencies exceeding 18%.[21]

Reccent research has highlighted that donor organic molecules incorporating B,N heterocyclic patterns can be synthesized in place via photochemical activation in solid polymer matrices, providing an efficient approach for engineering functional donor materials.[22]

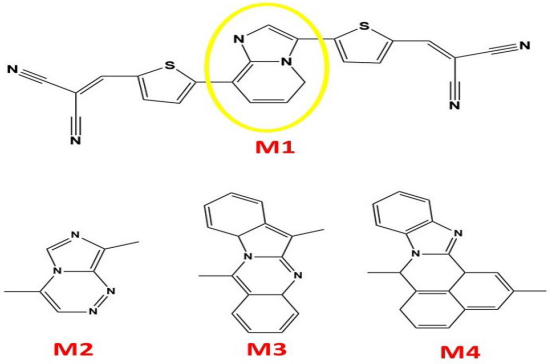

Fig. 1. Chemical structures of the investigated donor analogues M1-M4.

In this study, we designed and analyzed four N-fused heterocyclic small-molecule donor analogues (M1–M4) for comparative theoretical screening in organic solar cells. The selected molecular series was constructed to examine how variations in the central fused heterocyclic core influence frontier orbital energies, charge-transfer character, and light-harvesting behavior. These donor systems were designed from fused heterocyclic core motifs inspired by zolpidem-, temozolomide, and tryptanthrin-related frameworks, but structurally re-engineered for photovoltaic purposes. M3 and M4 share a tryptanthrin-related fused core, whereas M4 contains an additional fused aromatic ring relative to M3. In all cases, the central donor core was symmetrically functionalized with two 2-(2-thienylmethylene)malononitrile terminal units in

order to enhance π-conjugation and promote intramolecular charge transfer. These compounds were therefore investigated as designed donor analogues to establish structure–property relationships relevant to molecular photovoltaic.

2. Technical computation

In all calculations in our study on the spatial configuration and electronic properties of various molecules, calculations were performed using the Gaussian 09 software package.[23] The molecular geometries were initially constructed and fully optimized using the B3LYP (Becke three-parameter Lee-Yang-Parr) exchange-correlation functional, which is widely recognized for its accuracy in predicting electronic structures.[24] The 6-31G(d,p) basis set was employed for all atoms, including nitrogen (N), carbon (C), sulfur (S), and hydrogen (H).[25] Confirmation that all optimized structures correspond to true energy minima, with no imaginary frequencies observed, was achieved through frequency analysis at the same theoretical level. For the energy-level comparison, the HOMO and LUMO values of PCBM were taken from the literature and used as reference acceptor levels in the present study. To more accurately reproduce or predict experimental spectra, it is essential to account for solvent effects in theoretical calculations. The polarizable continuum model (PCM)[26] has emerged as one of the most effective methods for modeling bulk solvent environments for both ground and excited states.

In this work, the conductor-like polarizable continuum model (CPCM) was employed using tetrahydrofuran (THF) as the solvent environment.[24] THF was selected as a representative moderately polar aprotic solvent, providing a balanced dielectric medium for conjugated organic systems. Within the scope of the present study, this solvent model was used as a common reference environment to enable a consistent comparative evaluation of the investigated N-fused heterocyclic donor analogues. Accordingly, the computed optical and photovoltaic trends should be interpreted as relative structure-property relationships established under the same dielectric conditions. Time-dependent DFT (TD-DFT) calculations were performed on the optimized ground-state geometries to evaluate the excited-state energies and corresponding oscillator strengths. The global reactivity descriptors were estimated within the framework of conceptual DFT. The ionization potential and electron affinity were approximated as IP = $-E_{HOMO}$ and EA = $-E_{LUMO}$ respectively.[27-30] The electronegativity and chemical potential were calculated as $\boldsymbol{\chi} = \frac{\mathbf{1}}{\mathbf{2}}\ (\boldsymbol{EA} - \boldsymbol{IP}) = -\boldsymbol{\eta}$.[31-33] While the chemical hardness ($\boldsymbol{\eta}$), a measure of resistance to charge transfer is obtained through $\boldsymbol{\eta} = \frac{\mathbf{1}}{\mathbf{2}}\ (\boldsymbol{EA} + \boldsymbol{IP})$ [34], the softness was taken as $S = \frac{1}{2\eta}$ describing molecular polarizability.35-38 Finally, the electrophilicity index (ω) is a measure of electron deficient character guven by $\omega = \frac{\mu^2}{2\eta}$. [39-40]

The photovoltaic parameters discussed in this work were estimated using commonly employed comparative expressions for donor/acceptor systems in organic solar-cell screening studies. These equations were used here to compare the relative photovoltaic potential of the investigated donor analogues within a consistent theoretical framework. Accordingly, the obtained values should be interpreted as theoretical screening descriptors rather than as universally exact device-level predictions.

3. Results and analysis:

3.1 Electronic properties

The data presented in **Table 1** summarize the electronic and reactivity properties of the molecules M1-M4 after optimization calculations (**Fig. 2**). According to literature, the ideal HOMO energy level for donor molecules lies between -5.2 and -5.8 eV, while the optimal LUMO level ranges from -3.7 to -4.0 eV.[41] Molecules M2-M4 are located within the optimal HOMO energy level range and demonstrate that they could provide a sufficiently high open-circuit voltage, although the LUMO levels of molecular systems M1-M4 (from -3.05 to -3.46 eV) are located slightly above the recommended range, which may slightly diminish the electron-transfer driving force. Of all the molecules under investigation, M1 possesses the lowest HOMO energy (-4.729 eV) and the smallest bandgap (1.63 eV), suggesting better light-harvesting features and effective charge-carrier transformation. M4, instead, demonstrates the widest energy gap (2.591 eV), indicating that it can absorb more weakly in the visible to near-IR region. The calculated ionization potentials (IP) and electron affinities (EA) confirm the donor nature of all four molecules. Global reactivity descriptors provide additional insights, as M1 possesses the lowest S (0.613 eV) and μ (-3.914 eV), implying that it is the most reactive toward charge transfer.

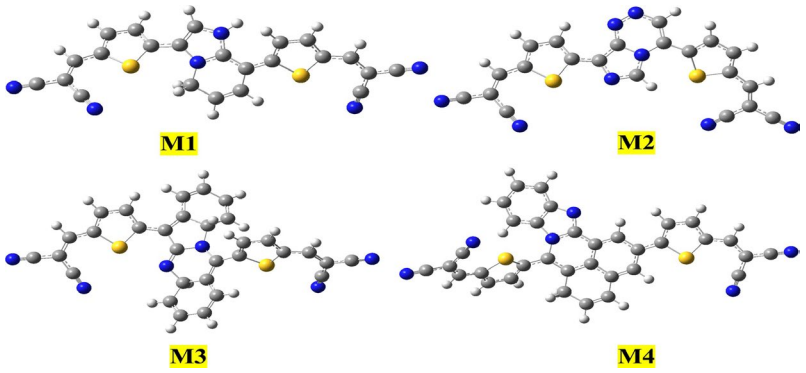

Fig. 2. Optimized geometries of the investigated donor analogues M1-M4.

From a conceptual DFT perspective, narrower band gaps and lower hardness values indicate higher electronic softness and greater charge-transfer propensity, whereas deeper frontier orbital energies are associated with enhanced energetic stabilization and can favor higher open-circuit voltage. This charge-transport performance of M3 and M4 can also be understood from their frontier molecular orbital (FMO) distributions displayed in **Fig. 3**. In all four molecules (M1-M4), the HOMO is mainly localized on the central conjugated core and donor system, suggesting favorable hole-transport possibilities. In contrast, the LUMO orbitals are primarily distributed on the electron-withdrawing acceptor arms, facilitating effective charge separation upon photoexcitation It is worth mentioning that M3 and M4 show significant orbital delocalization at both HOMO and LUMO levels, indicating enhanced pi-pi stacking and charge mobility, which are essential for efficient performance in donor-type organic solar cells.

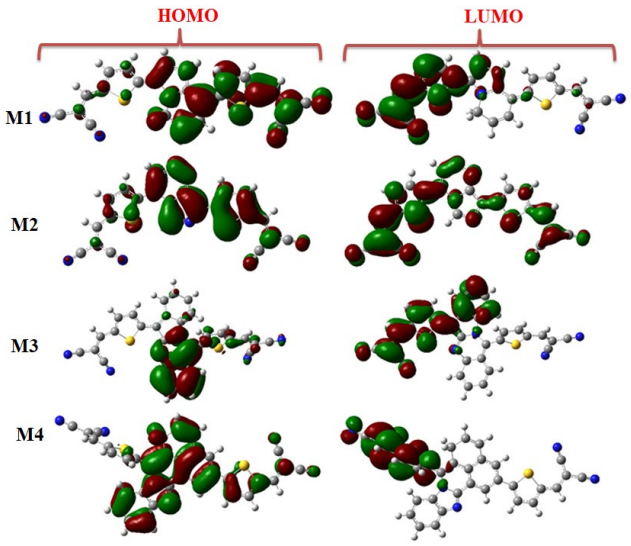

Fig. 3. HOMO and LUMO distributions and energy-level alignment of the investigated donor analogues M1-M4 relative to PCBM.

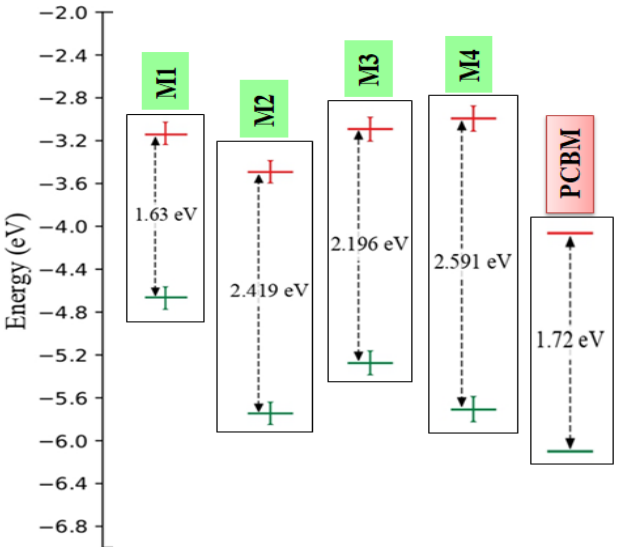

Fig. 4. HOMO/LUMO energy-level alignment of M1-M4 relative to PCBM.

Table 1. HOMO, LUMO, energy gap, ionization potential (IP), electron affinity (EA), and global reactivity parameters (μ, χ, η, S, and ω) of the investigated donor molecules

Molecules	M1	M2	M3	M4	PCBM-C60
E_{HOMO} (eV)	-4.729	-5.879	-5.274	-5.647	-6.02
E_{LUMO} (eV)	-3.099	-3.460	-3.078	-3.056	-4.3
E_{gap} (eV)	1.63	2.419	2.196	2.591	1.72
IP (eV)	4.729	5.879	5.274	5.647	6.02
EA (eV)	3.099	3.46	3.078	3.056	4.3
μ (eV)	-3.914	-4.6695	-4.176	-4.3515	-5.16
χ (eV)	3.914	4.6695	4.176	4.3515	5.16
η (eV)	0.815	1.2095	1.098	1.2955	0.86
S (eV)	0.613	0.413	0.455	0.386	0.581
ω (eV)	9.398	9.014	7.941	7.308	15.48

The energy-level alignment of the frontier molecular orbital levels for donor molecules M1-M4 and acceptor PCBM are depicted in Figure 4, providing essential structure-property relationships. All donor molecules exhibit higher HOMO energy levels than PCBM (-6.02 eV), with M1 showing the most favorable alignment (-4.73 eV) for efficient hole extraction. M2 (-5.88 eV) and M4 (-5.65 eV) fall within the optimal HOMO range for donor materials (between -5.2 and -5.8 eV). Although their LUMO energy levels (ranging from -3.05 to -3.46 eV) are significantly higher than that of PCBM (-4.3 eV), the electron injection process from the excited-state LUMO of the donor molecules to the LUMO of the acceptor (PCBM) remains energetically favorable.

4. Photovoltaic Properties

The power conversion efficiency (PCE) is the primary metric used to evaluate solar cell performance.[43] It is calculated using the following equation:

$$PCE = \frac{J_{SC}V_{OC}FF}{P_{Solar}} \quad (1)$$

where P_{Solar} indicates the incident power density, J_{SC} is the symbol of the current density at short-circuit, while V_{OC} stands for the voltage at open-circuit, and FF refers to the fill factor.

$$FF = \frac{v_{oc} - ln\,(v_{oc} + 0.72)}{v_{oc} + 1} \quad (2)$$

$$v_{oc} = \frac{eV_{OC}}{nK_BT} \quad (3)$$

where e denotes the elementary charge, V_{oc} represents the open-circuit voltage, T is the absolute temperature,and K_B is the Boltzmann constant. The v_{oc} values have been computed at n = 1, where n is the ideal factor for a diode.[44]

The maximum open-circuit voltage[45] is estimated by the following expression:

$$V_{OC} = \frac{1}{e}(|E_{HOMO}(Donor) - E_{LUMO}(Acceptor)|) - 0.3 \quad (4)$$

where 0.3 V is an empirical factor introduced by Scharber et al.[46-47]

For clarity, the photovoltaic parameters discussed below are based on comparative theoretical estimations introduced in the Computational Details section. The following discussion is therefore focused on the relative trends among the investigated compounds under the same modeling assumptions.

The V_{OC} values for M1 to M4 are listed in **Table 2**, which are respectively 0.129 V, 1.279 V, 0.674 V, and 1.047 V. The donors M2 and M4 show the highest V_{OC} values of 1.279 V and 1.047 V, respectively, suggesting the most favorable energetic alignment and the greatest potential for efficient photovoltaic performance. While M3 and M1 display a moderate open-circuit voltage, implying a less efficient charge transfer. **Fig.** 5 illustrates the variation of V_{OC} for all donor molecules M1-M4 using PCBM as the acceptor. The comparison of energy levels, HOMO, LUMO, band gap, and open-circuit voltage (Voc), suggests that M3 combines a moderate band gap with acceptable Voc, making it the most promising candidate.

Furthermore, the Fill Factor (FF) ranged between 0.542 and 0.903. It reflects the quality of the solar cell circuit, highlighting the differences in performance among the donors. Notably, M1 presents the donor corresponding to the highest FF (0.903), demonstrating the most favorable charge-transport properties.

Table 2. Electronic and photovoltaic characteristics of the donor molecules (M1-M5), including the dimensionless voltage, fill factor, αi factor, and open-circuit voltage (Voc).

Molecules	E_{LUMO} (eV)	E_{HOMO} (eV)	V_{OC} (V)	v_{OC}	FF
M1	-3.099	-4.729	0.129	4.990	0.5423
M2	-3.460	-5.879	1.279	49.487	0.9025
M3	-3.078	-5.274	0.674	26.070	0.8419
M4	-3.056	-5.647	1.047	40.509	0.8862

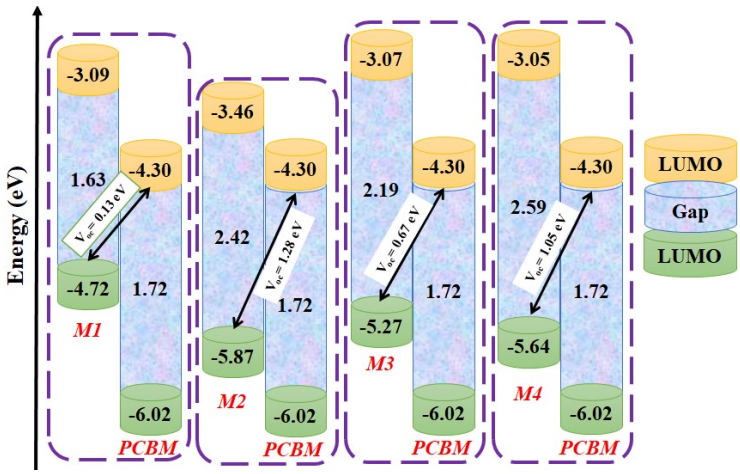

Fig. 5. Variation of open-circuit voltage (Voc) for all engineered donor molecules using PCBM as the acceptor material.

The density of the short-circuit current (J_{SC})[48] can be evaluated using:

$$J_{SC} = \int LHE(\lambda)\Phi_{inj}\xi_{collect}d\lambda \quad (5)$$

The light-harvesting efficiency is denoted by LHE(λ)[49]. To achieve maximum photocurrent, the LHE must be high, which can be expressed as:

$$LHE = 1 - 10^{-f} \quad (6)$$

The photovoltaic results in **Table 3** clearly show the importance of frontier orbital relative alignment on the performance of the D-A systems. The energy offset between the HOMO and LUMO levels governs both the open-circuit voltage (V_{OC}) as well as the ability of a system to efficiently dissociate excitons. Alignment is therefore important to facilitate charge transfer without energy loss. Therefore, tuning these molecular electronic energy levels is required to maximize the efficiency of organic solar cells as a whole.

Table 3. Photovoltaic properties and light-harvesting characteristics of the studied molecules (M1-M4) obtained at the B3LYP/6-31G(d,p) level with CPCM (THF) solvation.

Molecules	E_{LUMO} (eV)	E_{HOMO} (eV)	$L_D - L_A$ (eV)	*f*	*LHE*
M1	-3.099	-4.729	1.201	1.2854	0.790
M2	-3.460	-5.879	0.840	0.6774	0.790
M3	-3.078	-5.274	1.222	0.1503	0.292
M4	-3.056	-5.647	1.244	0.6578	0.780

For these four structures (M1-M4), M2 is the best candidate since it has the largest V_{OC} = 1.279 V, which can be ascribed to its deep HOMO (-5.879 eV) that reduces energy loss during charge separation. It also possesses a moderate LUMO offset (LD-LA = 0.840 eV), which guarantees efficient exciton dissociation. On the other hand, M1 possesses a high oscillator strength (f = 1.2854) and LHE (0.790), but its near-zero HOMO (-4.729 eV) could lead to an extremely small V_{OC} = 0.129 eV. M3 exhibits inferior light absorption (f = 0.1503, LHE = 0.292) and a reasonable V_{OC} = 0.674 V. M4 also shows strong absorption (f = 0.6578, LHE = 0.780), a high V_{OC} equal to 1.047 eV, and a relatively large LUMO offset of 1.244 eV, indicating the possibility of energy loss.

The Scharber plot is a commonly used tool to estimate power conversion efficiency (PCE) of organic photovoltaic (OPV) materials. It provides a plot-based method for estimating the ultimate attainable PCE of an OSC based on donor material energy levels, namely HOMO and LUMO energies, plus their alignment with a benchmark acceptor, which is generally [6,6]-phenyl-C61-butyrate methyl ester (PCBM).[50] In this regard, the HOMO-LUMO energy gap and the relative position of empty orbitals are important parameters that affect Voc, Jsc, and finally PCE. The Scharber plot of M1-M4 is depicted in Figure 6. This provides a useful framework for identifying which molecules are most worthwhile for further development in organic solar cells.

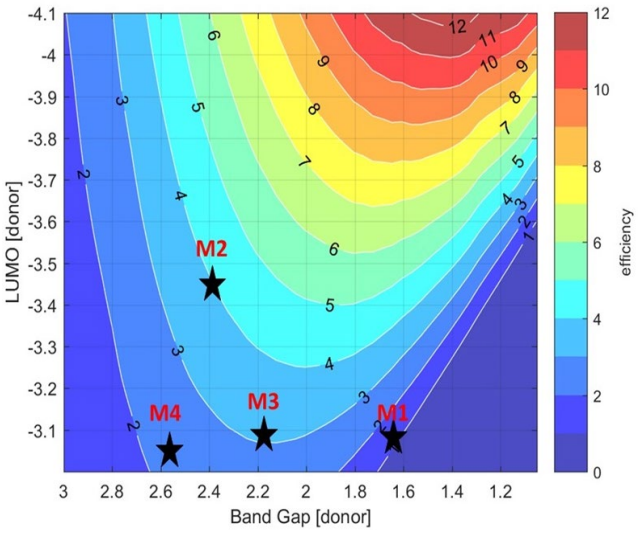

Fig. 6. Scharber diagram to estimate PCE (%) for all donor molecules M1-M4.

The PCEs of the donor molecules M1-M4 have been estimated. The obtained values are approximately 1% for M1, 4% for M2, 3% for M3, and 2% for M4. Among these complexes, M2 is particularly efficient in its performance of solar energy conversion to electricity. This is attributable to the favorable energy-level alignment of its HOMO and LUMO bands with those of the conventional acceptor. The relatively low efficiency of M1 indicates poor energy-level matching or an inappropriate energy gap. All of these results demonstrate that M2 is a promising candidate for organic solar cells.

5. Molecular Electrostatic Charge Potential (Mep) Analysis

The molecular electrostatic potential (MEP) provides a practical method for assessing nucleophile-electrophile interactions by visualizing the reactive regions of a molecule. Calculated at the B3LYP/6-31G(d,p) level with CPCM/THF solvation, the MEP surfaces of molecules M1-M4 display different spatial regions according to the electrostatic potential. As depicted in Figure 7, they possess complementary reactive sites, predicted as electrophilic reactivity in electron-poor regions and

nucleophilic reactivity in electron-rich regions. The electron-rich core with electronegative N termini contributes to the amphiphilic nature of the molecular system. This bimodal characteristic is conducive to both electron donation and electron acceptance in such molecules.[42]

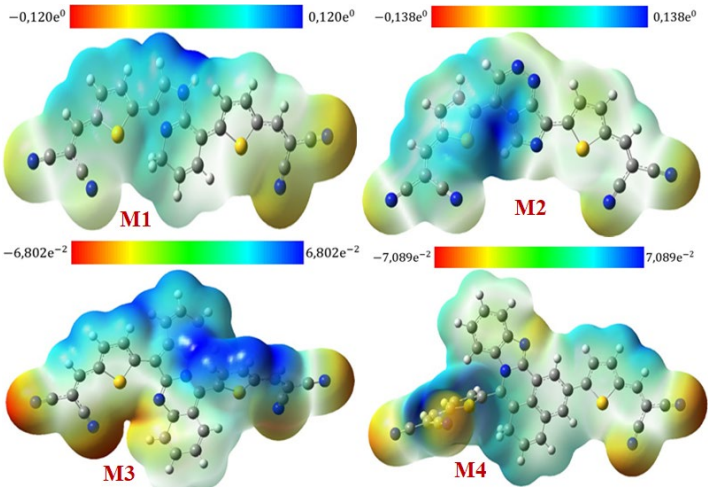

Fig. 7. MEP maps of all levels of the molecules under study.

As shown in **Fig. 7**, the molecular electrostatic potential (MEP) maps clearly demonstrate the charge distribution across molecules M1-M4. The red regions (negative potential) are predominantly located around the nitrogen atoms of the cyano groups and the sulfur-containing termini, indicating electron-rich areas prone to interaction with electrophilic species. In contrast, the blue regions (positive potential), especially over the fused core, correspond to electron-deficient zones resulting from intramolecular polarization.

A comparative analysis of the molecules highlights distinct features. M1 shows a fairly uniform and nearly symmetrical charge distribution, with moderate negative regions around heteroatoms, suggesting balanced reactivity. Conversely, M2 exhibits a pronounced and extended blue region in the central part of the molecule, indicating a strong electron-deficient nature and enhanced electrophilicity.

In the case of M3, the MEP map reveals stronger polarization, with a clear contrast between red and blue regions, pointing to the existence of multiple reactive sites. Lastly, M4 is characterized by a well-defined separation of charge, with highly localized positive and negative regions, indicating a markedly uneven charge distribution and more site-specific reactivity.

6. Density of States (DOS)

Density of states (DOS) analysis provides a graphical representation of the distribution of electronic states as a function of energy. In conjugated donor materials, DOS is useful for examining the density of occupied and unoccupied states around the frontier orbital region and for assessing how structural variations affect charge-transport-relevant electronic features.

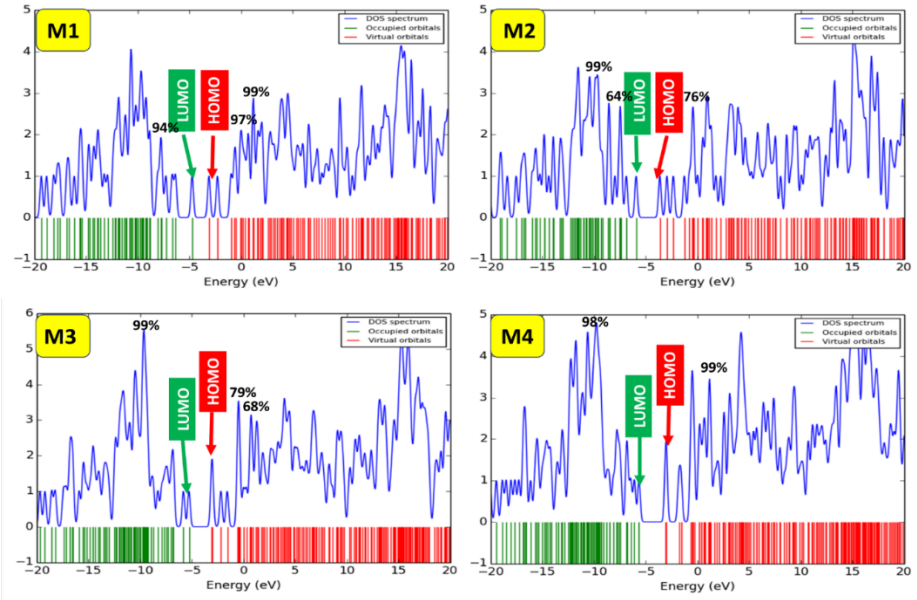

Fig. 8. Density of states (DOS) of the investigated donor molecules for photovoltaic applications.

Fig. 8 shows a DOS analysis evidencing differences in the basic electronic structure between donor molecules M1-M4. All donor molecules show typical semiconductor behavior, meaning that occupied (HOMO) and unoccupied (LUMO) states are clearly defined, although the resolution of energy distribution and state density differs. M1 has the best electronic structure for photovoltaic applications, possessing a narrow bandgap (Eg = 1.63 eV) and a high density of states close to the band edges due to closely spaced HOMO and LUMO orbitals, revealing good charge-transfer ability. The sharper peaks of M2 near the Fermi level indicate that more localized charge carriers are involved, which may lead to improved carrier transport. These DOS distributions are wider than those of M3 and M4 due to their extended pi-conjugation; however, this also results in larger bandgaps of 2.20 eV (M3)61 and 2.59 eV (M4)62, which can be detrimental to light absorption. It is noteworthy that states around the Fermi level show symmetric distribution in both directions across all molecules, suggesting good balanced carrier-transport abilities, which are an important condition for high-performance OSC materials. These DOS features correlate well with the performance of the molecules as donors and explain why M1 appears most favorable in this role, while M3 and M4 may be better suited for applications requiring bandgap-selective characteristics.

7. Absorption Analysis

The absorption spectra and electronic transitions of M1-M4 provide important structure-property relationships relevant for photovoltaics. As shown in **Fig. 9**, M1 exhibits the most intense and broadest absorption profile, extending from the visible to the near-infrared region (415-935 nm).

Table 4 demonstrates that M1's exceptional absorption breadth arises from three key transitions: (1) a HOMO→LUMO transition at 934.88 nm (f = 0.336), enabling NIR absorption, and (2) a particularly strong HOMO→L+1 transition at 536.94 nm (f = 1.2854). While all molecules display characteristic π-π* transitions, their absorption profiles differ significantly. M2 exhibits strong visible absorption (659.07 nm and 469.90 nm) but lacks NIR coverage, whereas M3 shows relatively weak yet well-defined peaks in the red region (685-727 nm). M4's absorption is concentrated in the 477-595 nm range, with its strongest transition at 538.55 nm (f = 0.6578).

Table 4. Calculated excitation parameters and main electronic transitions of M1-M4.

Molecules	Energy (eV)	Wavelength (nm)	*f*	Transition
	1.326	934.88	0.3360	HOMO → LUMO (100%)
M1	2.309	536.94	1.2854	HOMO → L+1 (97%)
	2.985	415.32	0.0528	H-1 → LUMO (94%)
	1.881	659.07	0.5648	HOMO → LUMO (99%)
M2	2.638	469.90	0.6774	HOMO → L+1 (76%)
	2.868	432.36	0.0507	H-2 → LUMO (64%)
	1.706	726.54	0.0036	HOMO → LUMO (98%)
M3	1.808	685.91	0.1503	HOMO → L+1 (99%)
	2.415	513.37	0.0050	H-1 → L+1 (99%)
	2.084	594.79	0.0032	HOMO → LUMO (98%)
M4	2.302	538.55	0.6578	HOMO → L+1 (99%)
	2.598	477.17	0.0013	H-1 → LUMO (100%)

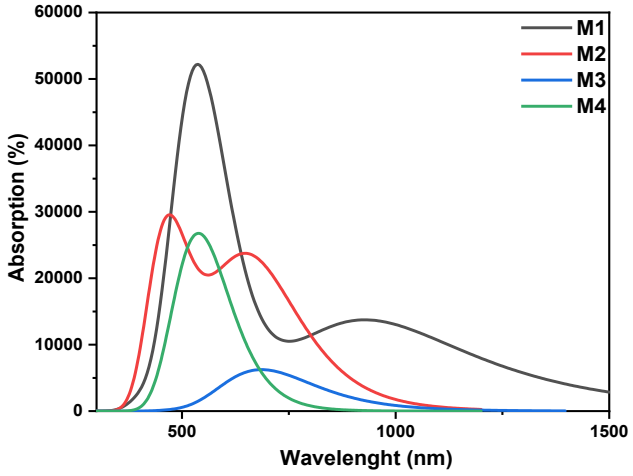

Fig. 9. Absorption spectra of donor molecules (M1-M4) obtained at the B3LYP/6-31G(d,p) level with CPCM (THF) solvation.

8. Conclusion

This theoretical investigation demonstrates that N-fused heterocyclic molecules (M1-M4) are promising organic donor molecules for organic solar cells (OSCs) due to their diverse electronic and optical properties. DFT and TD-DFT calculations

show that M1 has the smallest bandgap (1.63 eV), broad absorption from the visible to the near-infrared region, and high chemical softness, favoring efficient charge transfer, although its calculated PCE is limited to 1%. M2, with a lower HOMO (-5.88 eV) and a Voc of 1.28 V, achieves the highest PCE (4%), while M3 and M4 show intermediate performance (PCE values of 3% and 2%, respectively). Molecular electrostatic potential (MEP) analysis revealed amphiphilic reactivity, with electrophilic nuclei and nucleophilic end groups, suggesting dual donor-acceptor behavior favorable for charge transfer. These results indicate that N-fused heterocycles can be tuned and optimized to produce efficient donor materials. This study thus provides a solid theoretical basis to guide experimental research and the rational design of new organic materials with high photovoltaic performance.

References

[1] Kim S., Hoang V. Q., and Bark C. W. **(2021)** Silicon-based technologies for flexible photovoltaic (PV) devices: From basic mechanism to manufacturing technologies. *Nanomaterials*, 11(11), 2944. (https://doi.org/10.3390/nano11112944).

[2] Tanko K. T., Tian Z., Raga S., Xie H., Katz E. A., and Lira-Cantu M. **(2025)** Stability and reliability of perovskite photovoltaics: Are we there yet? *MRS Bull.,* 50(4), 512-525. (https://doi.org/10.1557/s43577-025-00863-5).

[3] Lin C., Peng R., Song W., Gao J., Feng T., Bai Y., and Ge Z. **(2025)** Enhancing mechanical durability and long-term stability in organic solar cells via flexible linker-sequential block copolymerized donors. *Angew. Chem. Int. Ed.,* 64(7), e202420121. (https://doi.org/10.1002/anie.202420121).

[4] Rafique S., Abdullah S. M., Sulaiman K., and Iwamoto M. **(2018)** Fundamentals of bulk heterojunction organic solar cells: An overview of stability/degradation issues and strategies for improvement. *Renew. Sustain. Energy Rev.,* 84, 43-53. (https://doi.org/10.1016/j.rser.2017.12.008).

[5] Søndergaard R.R., Hösel M., Krebs F.C. **(2013)** Roll-to-roll fabrication of large area functional organic materials. *J. Polym. Sci. B Polym. Phys.,* 51(1), 16-34. (https://doi.org/10.1002/polb.23192).

[6] Zouitina S., Aboulouard A., Ghazali A. E., Tounsi A., El idrissi M. **(2023)** Computational study of new thiophene-based small molecules as donor materials for bulk heterojunction photovoltaic cells. *J. Fluoresc.,* 33(2), 553-563. (https://doi.org/10.1007/s10895-022-03077-z.

[7] Tong Y., Xiao Z., Du X., Zuo C., Li Y., Lv M., Yuan Y., Yi C., Hao F., Hua Y., Lei T., Lin Q., Sun K., Zhao D., Duan C., Shao X., Li W., Yip H. L., Xiao Z., Zhang B., Bian Q., Cheng Y., Liu S., Cheng M., Jin Z., Yang S., and Ding L. **(2020)** Progress of the key materials for organic solar cells. *Sci. China Chem.,* 63(6), 758-765. (https://doi.org/10.1007/s11426-020-9726-0).

[8] Von Hauff E., Dyakonov V., Parisi J. **(2005)** Study of field effect mobility in PCBM films and P3HT:PCBM blends. *Sol.Energy Mater. Sol. Cells.,* 87(1-4), 149-156. (https://doi.org/10.1016/j.solmat.2004.06.014.

[9] Aboulouard A., Gürek A. G., El idrissi M. **(2021)** Computational study of organic small molecules based on imidazolinone for photovoltaic applications. *Energy Sources, Part A.,* 43(20), 2583-2594. (https://doi.org/10.1080/15567036.2020.1827092).

[10] Kim H. Y., Choi M. H., Han Y. W., Moon D. K., and Haw J. R. **(2016)** Deep HOMO polymers comprising anthracene units for bulk heterojunction solar cells. *J. Ind. Eng. Chem.,* 33, 209-220. (https://doi.org/10.1016/j.jiec.2015.10.010).

[11] Zou Y., Holmes R. J. **(2015)** Correlation between the open-circuit voltage and charge transfer state energy in organic photovoltaic cells. *ACS Appl. Mater. Interfaces.,* 7 (33), 18337-18342. (https://doi.org/10.1021/acsami.5b03656).

[12] Aboulouard A., Demir N., Can M., El idrissi M. **(2023)** Electronic and optical aspects of novel quinoxaline derivatives as electron donor materials for bulk heterojunction solar cells. *J. Mol. Graph. Model.,* 121, 108462. (https://doi.org/10.1016/j.jmgm.2023.108462).

[13] Ouhrir J., Mekaoui Y., Mennas I., Taj S., El Idrissi M., Manaut B. **(2025)** Exploring the optoelectronic and photovoltaic potential of Spiro-OMeTAD derivatives through quantum chemical investigations. *Curr. Chem. Lett.,* 14, 885-896. (https://doi.org/10.5267/j.ccl.2025.9.001).

[14] Taylor R. D., MacCoss M., Lawson A. D. **(2014)** Rings in drugs. *J. Med. Chem.,* 57 (14) 5845-5859. (https://doi.org/10.1021/jm4017625).

[15] Ning J., Tian Z., Wang B., Ge G., An Y., Hou J., Wang C., Zhao X., Li Y., Tian X., Yu Z., Huo X., Sun C., Feng L., Cui J., Ma X. **(2018)** A highly sensitive and selective two-photon fluorescent probe for real-time sensing of cytochrome P450 1A1 in living systems. *Mater. Chem. Front.,* 2, 2013-2020. (https://doi.org/10.1039/C8QM00372F).

[16] Kumar S., Bawa S., Gupta H. **(2009)** Biological activities of quinoline derivatives. *Mini-Rev. Med. Chem.,* 9(14), 1648-1654. (https://doi.org/10.2174/138955709789878001).

[17] Bollini M., Casal J. J., Alvarez D. E., Boiani L., González M., Cerecetto H., Bruno A. M. **(2009)** New potent imidazoisoquinolinone derivatives as anti-Trypanosoma cruzi agents: Biological evaluation and structure-activity relationships. *Bioorg. Med. Chem.,* 17, 1437-1444. (https://doi.org/10.1016/j.bmc.2009.01.011).

[18] Cui J., Gao G., Zhao H., Liu Y., Nie H., and Zhang X. **(2017)** A highly sensitive and selective fluorescent probe for N2H4 in air and living cells. *New J. Chem.,* 41, 11891-11897. (https://doi.org/10.1039/C7NJ01943B).

[19] Hao Y., Guo J., Wang Z., Liu Y., Li Y., Ma D., Wang Q. **(2020)** Discovery of tryptanthrins as novel antiviral and anti-phytopathogenic-fungus agents. *J. Agric. Food Chem.,* 68(20), 5586-5595. (https://doi.org/10.1021/acs.jafc.0c02101).

[20] Zong H.-H., Yao C., Sun C. Q., Zhang J.-G., Zhang L. **(2020)** Structure and stability of aromatic nitrogen heterocycles used in the field of energetic materials. *Molecules.,* 25(14), 3232. (https://doi.org/10.3390/molecules25143232).

[21] Vitaku E., Smith D. T., Njardarson J. T. **(2014)** Analysis of the structural diversity, substitution patterns, and frequency of nitrogen heterocycles among U.S. FDA approved pharmaceuticals. *J. Med. Chem.,* 57(24), 10257-10274. (https://doi.org/10.1021/jm501100b).

[22] Wang J., Zhan X. **(2021)** Fused-ring electron acceptors for photovoltaics and beyond. Acc. Chem. Res., 54 (1) 132-143. (https://doi.org/10.1021/acs.accounts.0c00721).

[23] Lu J.-S., Ko S.-B., Walters N. R., Kang Y., Sauriol F., Wang S. **(2013)** Formation of azaborines by photoelimination of B,N-heterocyclic compounds. *Angew. Chem. Int. Ed.,* 52(21), 5645-5648. (https://doi.org/10.1002/anie.201300829).

[24] Aboulouard A., Demir N., Can M., El idrissi M. **(2023)** Electronic and optical aspects of novel quinoxaline derivatives as electron donor materials for bulk heterojunction solar cells. *J. Mol. Graph. Model.,* 121, 108462. (https://doi.org/10.1016/j.jmgm.2023.108462).

[25] R. Diany, S. Kerraj, M.K Atouailaa, A. Arif, A. Aboulouard, M. Boulghalate, M. Salah and El idrissi M. **(2025)** Enhancing the electronic and optical performance of dye-sensitized solar cells with alizarin-based dyes: DFT/TDDFT investigations. *Current Chemistry Letters*., 14, 597–612. (https://doi.org/10.5267/j.ccl.2025.2.006).

[26] Becke A. D. **(1993)** Density-functional thermochemistry. III. The role of exact exchange. *J. Chem. Phys.,* 98(7), 5648-5652. (https://doi.org/10.1063/1.464913).

[27] Tomasi J., Mennucci B., and Cammi R. **(2005)** Quantum mechanical continuum solvation models. *Chem. Rev.,* 105(8), 2999-3094. (https://doi.org/10.1021/cr9904009).

[28] Takano Y., Houk K. N. **(2005)** Benchmarking the conductor-like polarizable continuum model (CPCM) for aqueous solvation free energies of neutral and ionic organic molecules. *J. Chem. Theory Comput.,* 1(1), 70-77. (https://doi.org/10.1021/ct049977a).

[29] Parr R. G., Donnelly R. A., Levy M., Palke W. E. **(1978)** Electronegativity: The density functional viewpoint. *J. Chem. Phys.,* 68, 3801-3807. (https://doi.org/10.1063/1.436185).

[30] Parr R. G., Pearson R. G. **(1983)** Absolute hardness: Companion parameter to absolute electronegativity. *J. Am. Chem. Soc.,* 105, 7512-7516. (https://doi.org/10.1021/ja00364a005).

[31] Pearson R. G. **(1988)** Absolute electronegativity and hardness: Applications to inorganic chemistry. *Inorg. Chem.,* 27, 734-740. (https://doi.org/10.1021/ic00277a030).

[32] Putz M. V., Russo N., Sicilia E. **(2005)** About the Mulliken electronegativity in DFT. *Theor. Chem. Acc.,* 114, 38-45. (https://doi.org/10.1007/s00214-005-0657-9).

[33] Vijayaraj R., Subramanian V., Chattaraj P. K. **(2009)** Comparison of global reactivity descriptors calculated using various density functionals: A QSAR perspective. *J. Chem. Theory Comput.,* 5, 2744-2753. (https://doi.org/10.1021/ct900207u).

[34] Khalid M., Khan M. U., Azhar N., Arshad M. N., Asiri A. M., Braga A. A. C., Akhtar M. N. **(2022)** Exploration of nonlinear optical enhancement and interesting optical behavior with pyrene moiety as the conjugated donor and efficient modification in acceptor moieties. *Opt. Quantum Electron.,* 54(7), 395. (https://doi.org/10.1007/s11082-022-03782-w).

[35] Atouailaa M. K., Aboulouard A., Zeroual A., Syed A., Boulghalat M., Can M., El idrissi M. **(2025)** Surveying novel pyrazine acceptor materials for bulk heterojunction solar cells: Computational insights into photovoltaic performance. *J. Fluoresc.,* 35, 11273-11285. (https://doi.org/10.1007/s10895-025-04371-2).

[36] Parr R. G., Szentpály L. V., Liu S. **(1999)** Electrophilicity index. *J. Am. Chem. Soc.,* 121, 1922-1924. (https://doi.org/10.1021/ja983494x).

[37] Aboulouard A., Atouailaa M. K., Elhadadi B., Bensemlali M., Boulghallat M., Laasri S., El idrissi M. **(2022)** A theoretical study of non-fullerene electron acceptor-based on thiophene derivatives for organic solar cells. *Mater. Today Proc.,* 66, 329-334. (https://doi.org/10.1016/j.matpr.2022.05.426).

[38] Arif A., Boukili B., Atouailaa M.K., Mennas I., El. Benharaf M., Zeroual A., El idrissi M. **(2026)** TD-DFT investigation of N,N-diphenylaniline-based organic dye adsorption on TiO_2 surfaces for dye-sensitized solar cells. *Current Chemistry Letters.,* 15**,** 355-368. (https://doi.org/10.5267/j.ccl.2026.1.002).

[39] Aboulouard A., Arif A., Can M., El idrissi M. **(2024)** Engineering quinoxaline-based non-fullerene acceptors for high-performance organic solar cells: A DFT and TD-DFT study. *Mater. Chem. Phys.,* 310, 127993. (https://doi.org/10.1016/j.matchemphys.2024.127993).

[40] Shi G. Z., Wang Y. K., and Yuan Z. C. **(2016)** Dopant-free spiro-triphenylamine/fluorene hole-transporting material for perovskite solar cells. *Adv. Funct. Mater.,* 26 (9), 1375-1381. (https://doi.org/10.1002/adfm.201504392).

[41] Blouin N., Michaud A., Gendron D., Wakim S., Blair E., Neagu-Plesu R., Bellette M., Durocher G., Tao Y., and Leclerc M. **(2008)** Toward a rational design of poly(2,7-carbazole) derivatives for solar cells. *J. Am. Chem. Soc.,* 130(2), 732-742. (https://doi.org/10.1021/ja0771989).

[42] Albayati R., Kansız S., Dege N., Kaya S., Marzouki R., Lgaz H., Salghi R., Ali I. H., Alghamdi M. M., Chung I.-M. **(2020)** Synthesis, crystal structure, Hirshfeld surface analysis and DFT calculations of 2-[(2,3-dimethylphenyl)amino]-N′-[(E)-thiophen-2-ylmethylidene]benzohydrazide. *J. Mol. Struct.,* 1205, 127654. (https://doi.org/10.1016/j.molstruc.2019.127654).

[43] Albayati M. R., Kansız S., Dege N., Kaya S., Marzouki R., Lgaz H., Salghi R., Ali I. H., Alghamdi M. M., and Chung I.-M. **(2020)** Synthesis, crystal structure, Hirshfeld surface analysis and DFT calculations of 2-[(2,3-dimethylphenyl)amino]-N′-[(E)-thiophen-2-ylmethylidene]benzohydrazide. *J. Mol. Struct.,* 1205, 127654. (https://doi.org/10.1016/j.molstruc.2019.127654).

[44] Zhao C., Zhang Q., Zhou K., Ge H., Wang W., Yin S. **(2016)** Theoretical prediction on photovoltaic properties of 4Cl-BPPQ/PC61BM system via density functional theory calculations. *Chin. J. Chem.,* 34(11), 1143-1150. (https://doi.org/10.1002/cjoc.201600146).

[45] El Ghazali A., Aboulouard A., Gultekin B., El idrissi M. **(2023)** Theoretical investigation of novel electron donors for bulk heterojunction solar cells with potential photovoltaic characteristics. *J. Mol. Graph. Model*., 124, 108622. (https://doi.org/*10.1016/j.jmgm.2023.108622)*.

[46] Wu Z., Fan B., Xue F., Adachi C., Ouyang J. **(2010)** Organic molecules based on dithienyl-2,1,3-benzothiadiazole as new donor materials for solution-processed organic photovoltaic cells. Sol. *Energy Mater. Sol. Cells,* 94 (12), 2230-2237. (https://doi.org/10.1016/j.solmat.2010.07.023).

[47] Scharber M. C., Mühlbacher D., Koppe M., Denk P., Waldauf C., Heeger A. J., Brabec C. J. (2006) Design rules for donors in bulk-heterojunction solar cells towards 10% energy-conversion efficiency. *Adv. Mater.,* 18 (6), 789-794. (https://doi.org/10.1002/adma.200501717).

[48] Hachi M., Slimi A., Fitri A., El Khattabi S., Benjelloun A. T., Benzakour M., Mcharfi M. **(2020)** New small organic molecules based on thieno[2,3-b]indole for efficient bulk heterojunction organic solar cells: A computational study. *Mol. Phys.,* 118(8), e1662956. (https://doi.org/10.1080/00268976.2019.1662956).

[49] Ahmed S., Mushahary B. C., Kalita D. J. **(2020)** Rational design of bay-annulated indigo (BAI)-based oligomers for bulk heterojunction organic solar cells: A density functional theory study. *ACS Omega.,* 5, 8321-8333. (https://doi.org/10.1021/acsomega.0c00195).

[50] Aboulouard A., Mtougui S., Demir N., Moubarik A., El idrissi M., Can M. **(2021)** New nonfullerene electron acceptors based on quinoxaline derivatives for organic photovoltaic cells: DFT computational study. *Synth. Met.,* 279, 116846. (https://doi.org/10.1016/j.synthmet.2021.116846).

© 2026 by the authors; licensee Growing Science, Canada. This is an open access article distributed under the terms and conditions of the Creative Commons Attribution (CC-BY) license (http://creativecommons.org/licenses/by/4.0/).